Photo-double-ionization mechanisms in aromatic hydrocarbons

T. Hartman,[1] P. N. Juranić,[1,*] K. Collins,[2] B. Reilly,[3] E. Makoutz,[4] N. Appathurai,[1] and R. Wehlitz[1,†]

[1]*Synchrotron Radiation Center, University of Wisconsin–Madison, Stoughton, Wisconsin 53589, USA*

[2]*College of Education, Purdue University, West Lafayette, Indiana 47907, USA*

[3]*Department of Physics and Astronomy, University of Wisconsin–Madison, Madison, Wisconsin 53706, USA*

[4]*Michigan Technological University, Houghton, Michigan 49931, USA*

(Received 11 March 2013; published 5 June 2013)

We have measured the ratios of doubly to singly charged molecular parent ions of benzene (partially deuterated), naphthalene, anthracene, pentacene, pyrrole, furan, selenophene, and coronene for photon energies ranging from threshold to the carbon K shell. The photon-energy dependence of the ratio curves has been analyzed and compared to each other for the above molecules. We conclude that two—and in some cases three—different photo-double-ionization mechanisms exist for aromatic hydrocarbons. One of the mechanisms is the formation of a two-electron pseudoparticle. This finding may be useful in the quest for understanding high-temperature superconductivity.

DOI: 10.1103/PhysRevA.87.063403 PACS number(s): 33.80.Eh

I. INTRODUCTION

Direct photo-double-ionization, also known as direct double photoionization in the literature, of atoms in which two electrons are simultaneously emitted is of high interest for understanding electron correlations. Many investigations of photo-double-ionization have focused on helium—the textbook example for double ionization. Other atoms (see, e.g., [1,2]) and small molecules (see, e.g., [3–5]) have been investigated as well. However, the photo-double-ionization process in larger molecules consisting of more than six atoms has been investigated only marginally. There are only a few papers about doubly charged ions of benzene [4,30,31] and benzene clusters [6], and about doubly charged ions of larger hydrocarbons [7–10].

It is also worthwhile to mention a few investigations on the photo-double-ionization process in C_{60} that were performed over a larger photon energy range [11–13] or around the carbon K edge (i.e., the 1s ionization threshold) [14]. The C_{60} photo-double- to photo-single-ionization ratio exhibited a modulation extending from threshold to the carbon K edge that could be attributed to the particular structure of the C_{60} molecule [13], but it was not clear whether this modulation was a more general phenomenon.

In this paper, we will address the question of how the structure of an aromatic molecule affects the photo-double-ionization process for photon energies from threshold to the carbon K edge. Some of the results presented in this paper have already been published [15,16]. The goal of this paper is to provide more details and to also extend the energy range of the previously published data. Moreover, selenophene will serve as an example of how to apply our newly gained knowledge about photo-double-ionization mechanisms.

The motivation for our investigations is twofold and can be characterized by the following problems: (a) How do electrons move through large molecules such as biomolecules? How does the molecule react to this charge migration? (b) As outlined in Ref. [16], our investigations may help in the future to understand the underlying mechanisms in high-temperature superconductors [17], and in particular organic hydrocarbons [18] such as picene [19].

The idea of organic superconductors has already been discussed many years ago (see, e.g., [20–22]). In particular, aromatic hydrocarbons with their freely movable π electrons, which can behave similarly to superconduction electrons, are promising candidates, and pair correlation in molecules such as ovalene has been discussed [21]. Here, we offer a starting point for studying the pairing mechanism for high-temperature superconductivity from a molecular point of view, a mechanism that may or may not be based on electron-phonon coupling. Here we explore an alternative avenue for investigating this issue.

II. EXPERIMENT

Two different beamlines at the Synchrotron Radiation Center (SRC) in Stoughton, WI (USA) have been used in this investigation. The experiments were performed on the 6-m toroidal-grating monochromator (6m-TGM) beamline [23] with a bending-magnet source for photon energies from 17 to 170 eV and the varied line-spacing plane-grating monochromator (VLS-PGM) beamline with an undulator source [24] for energies from 150 to 280 eV. On the 6m-TGM we employed an Sn filter (17–36 eV), an Al filter (36–71 eV), an Si−3N−4 filter (71–100 eV), and a C filter (150–170 eV) to suppress higher-order and stray light. On the VLS we employed a C filter.

Because a high photon-energy resolution was not essential in these experiments, the entrance and exit slits were adjusted such that dead time of the detection electronics was not an issue. Generally, the slits were set as narrow as reasonably possible to avoid scattered light (in addition to using filters), but at the same time wide enough to get a decent signal.

The monochromatic photon beam entered through a differential pumping stage into the interaction region inside the vacuum chamber where the beam crossed the target molecules. A pulsed electric field accelerated the photoions

*Present address: Paul Scherrer Institute, CH-5232 Villigen, Switzerland.

†rwehlitz@src.wisc.edu

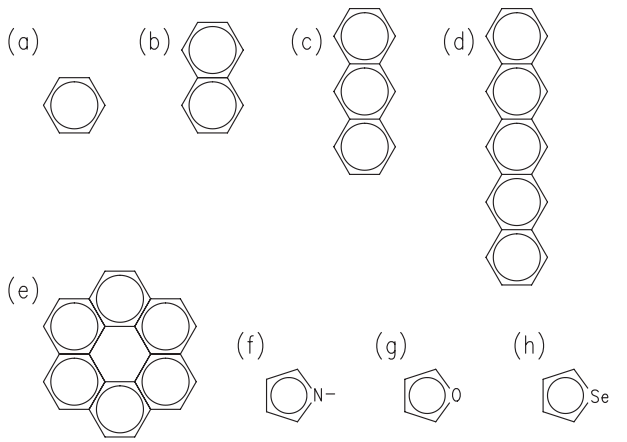

FIG. 1. The molecules studied in this investigation. (a) Partially deuterated benzene, (b) naphthalene, (c) anthracene, (d) pentacene, (e) coronene, (f) pyrrole, (g) furan, and (h) selenophene.

and photofragments toward a drift tube with a Z stack of microchannel plates (MCPs) at its end. The pulse period was 0.1 ms so that only long-lived metastable or fully stable ions were detected. A more detailed description of the setup can be found elsewhere [25].

We have detected doubly and singly charged molecular parent ions of partially deuterated benzene ($C_6H_3D_3$, Sigma-Aldrich, 98%purity), naphthalene ($C_{10}H_8$, Alfa-Aesar, 99.6% purity), anthracene ($C_{14}H_{10}$, Alfa-Aesar, 99.9%purity), pentacene ($C_{22}H_{14}$, Alfa-Aesar, 99.9%purity), pyrrole (C_4H_5N, Sigma-Aldrich, 98% purity), furan (C_4H_4O, Alfa-Aesar, 99% purity), selenophene (C_4H_4Se, Sigma-Aldrich, 97% purity), and coronene ($C_{24}H_{12}$, Sigma-Aldrich, 97%purity). The molecules' structures are displayed in Fig. 1 for reference. The reason why we have used *partially deuterated* benzene is that the fragment $C_3H_3^+$ and the doubly charged parent ion $C_6H_6^{2+}$ have the same mass-to-charge ratio and cannot be separated in our spectrometer, whereas $C_6H_3D_3^{2+}$ does not have a corresponding fragment of the same mass-to-charge ratio. The other molecules did not exhibit this problem.

The voltage across all three MCPs was set high enough, so that no discrimination between the doubly and singly charged ions was detectable. Figure 2 shows the ratio for anthracene and furan as a function of the MCP voltage. As one can see, the optimal MCP voltage is not always the same but also depends on the age of the MCPs.

Likewise, the threshold for processing a signal in the electronics was set low in the constant fraction discriminator (CFD) (Fig. 3) such that noise was suppressed without discriminating against different charge states. Note that different charge states have different signal strengths (pulse heights). Both settings, the MCP voltage and the CFD threshold, are important as they affect directly the ratio of doubly to singly charged ions.

It is worthwhile to mention that it was possible to have a low count rate of ions without any synchrotron light. This was due to (a) the ambient light in the experimental hall and (b) to the ion gauge monitoring the pressure of the vacuum chamber. The former was eliminated by covering all window flanges and the latter by turning the ion gauge off during data taking. Figure 4 shows an example of a partially deuterated benzene

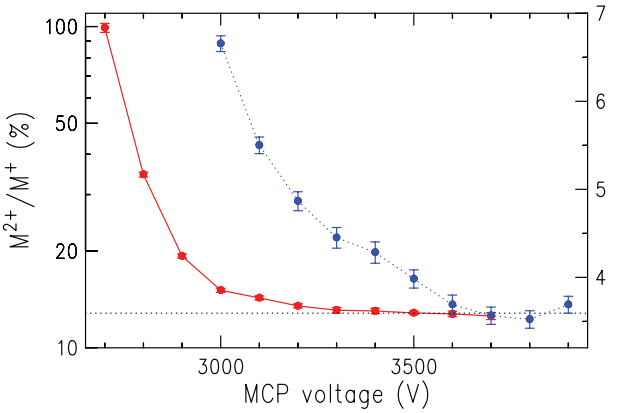

FIG. 2. (Color online) Photo-double- to photo-single-ionization ratio of anthracene (LH scale) and furan (RH scale) as a function of the MCP voltage U.

spectrum taken without light but with the ion gauge on and the same spectrum taken with light.

The liquid samples were freeze-pump-thawed three times to remove gases from the vial holding the sample. The vial containing the powder naphthalene was pumped for about 30 min before use. The powder anthracene had to be warmed up in a crucible to 33 °C to achieve a sufficient vapor pressure. Pentacene and coronene were vaporized using a resistively heated oven at a temperature of about 185 and 134 °C, respectively. The chamber's base pressure was in the mid-10^{-9}-mbar range. The sample gas pressure was about 1.0×10^{-6} mbar. A pressure dependence of the ratio could not be found in the pressure range used as demonstrated in Fig. 5. To get reliable results even at low gas pressures when the signal is weak, we have used a low mass-to-charge region ($m/q = 35$–45) denoted as "L" and a high mass-to-charge region ($m/q = 75$–85) denoted as "H" to monitor the L/H ratio as a function of gas pressure.

III. DATA ANALYSIS

We extracted the areas of the singly and doubly charged ion peaks in our ion time-of-flight spectra using direct numerical integration when possible. For some of the spectra we had to

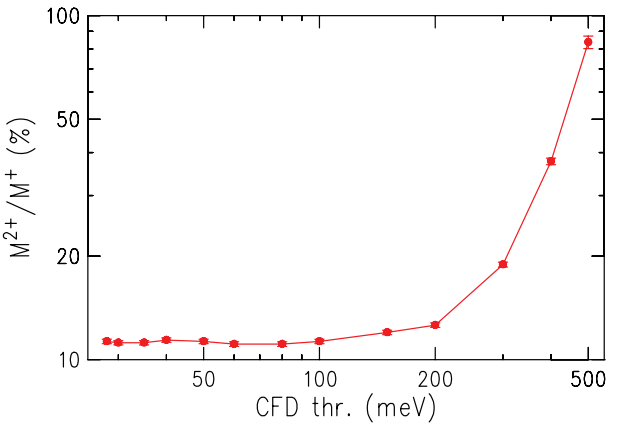

FIG. 3. (Color online) Photo-double- to photo-single-ionization ratio of anthracene as a function of the CFD threshold T_{CFD}.

fit the ion peaks if they were not separated from neighboring fragment peaks using a Voigt profile. In these cases, we determined the shape of the fragment peaks from a spectrum taken below the double-ionization threshold and kept the widths of the fragment peaks fixed for all other fits in order to minimize systematic errors.

As an example for this data analysis, we show the region of the doubly charged parent ion of deuterated benzene in Fig. 6. At that time our spectrometer' resolution was not as good as in later experiments with the other molecules due to a lower pusher voltage in the time-of-flight spectrometer. Nevertheless, the peak of doubly charged ions can be easily fitted keeping the shapes of the fragment peaks fixed. The shape of the fragment peaks was determined below the double-ionization threshold.

The calculated ratio R_s of doubly to singly charged parent ions pertains only to stable or long-lived metastable parent ions. It is well known that molecules can also dissociate into singly and doubly charged fragments after photoionization. Those fragments are clearly visible in our spectra but were not considered in this investigation. Instead, we focused on the parent ions that cannot be created by dissociation processes. One can disentangle the dissociative pathways for small molecules using photoelectron-photoion-photoion coincidences (see, e.g., [3,26–28]), but it is difficult to do so for large molecules. Thus, the ratio of the true photo-double- to photo-single-ionization cross sections will be different due to fragmentation processes. We note in passing that the photo-double- to photo-single-ionization ratio for benzene at 75 eV is about five times larger when measuring the photoelectrons instead of the photoions. This large difference is most likely due to the long flight time of the doubly charged ions that can fragment before reaching the detector and are, thus, not counted in the ion spectrum. An overview of the photoionization dynamics in molecules can be found in [29]. The numbers of doubly and singly charged *parent* ions are most likely to be larger right after photoionization than at the time when the ions are detected (about 100 μs later) after fragmentation has occurred. In this respect, our measured ratio is a simplified photo-double- to photo-single-ionization ratio for molecules, which can be determined reliably in a straightforward manner.

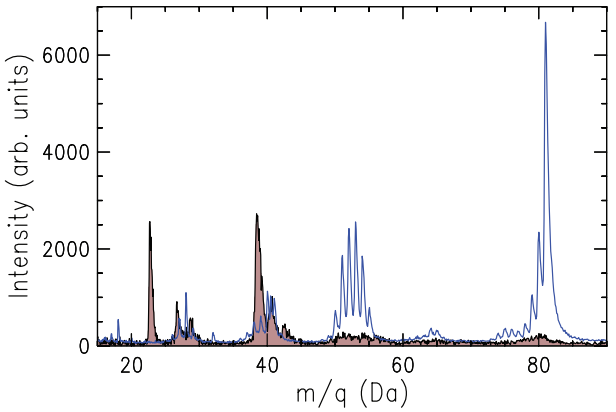

FIG. 4. (Color online) Ion spectra of partially deuterated benzene as a function of the mass-to-charge ratio. The solid line is a spectrum taken at 72 eV; the filled spectrum was taken without light but with the ion gauge turned on. The collection time for both spectra was the same.

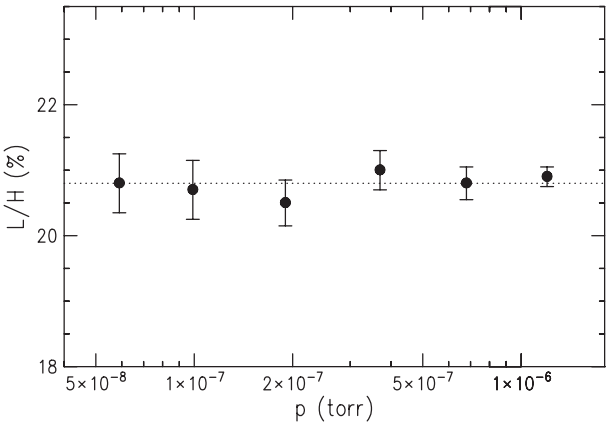

FIG. 5. Ratio of the low-to-high mass-to-charge ratio as a function of the chamber pressure for partially deuterated benzene.

The photon energy calibration of the 6m-TGM was accomplished with the help of the Ar $3s \rightarrow 4p$ resonance (in first and second order), the Ne $2s \rightarrow 3p$ resonance, the He $1s^2 \rightarrow 2s2p$ resonance, the Xe $4d \rightarrow 6p$ resonance, and the Kr $3d \rightarrow 5p$ resonance. On the VLS-PGM beamline, the Ar $2p_{3/2} \rightarrow 4s$ resonance has been used for energy calibration.

IV. RESULTS AND DISCUSSION

A. Low-energy region

Figure 7 shows the ratios R_s of doubly to singly charged parent ions near threshold of the molecules under investigation. To determine the double-ionization thresholds of the molecules, we applied a least-squares fit to the near-threshold ratios using a power function:

$$R_s(h\nu) = a(h\nu - E^{2+})^n + b. \quad (1)$$

Here, $h\nu$ is the photon energy, E^{2+} is the threshold energy, a is a fit parameter, n is an exponent, and b is an additional offset.

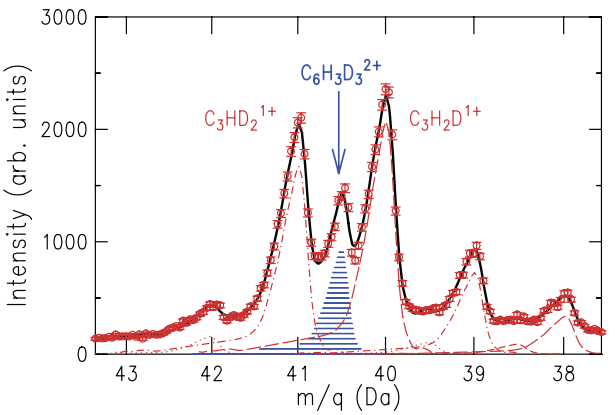

FIG. 6. (Color online) Part of an ion time-of-flight spectrum of deuterated benzene along with fit curves as a function of the mass-to-charge ratio taken at 37 eV. The gray (blue) shaded area is the doubly charged parent ion between two major fragments.

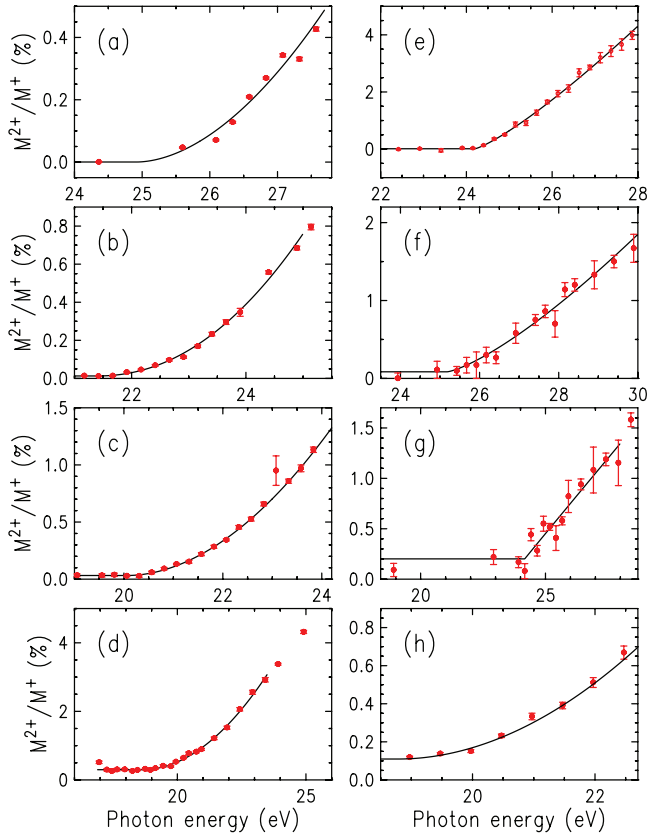

FIG. 7. (Color online) Ratio of doubly to singly charged parent ions R_s of (a) partially deuterated benzene, (b) naphthalene, (c) anthracene, (d) pentacene, (e) pyrrole, (f) furan, (g) selenophene, and (h) coronene. The solid lines are fit curves to determine the double-ionization threshold.

This empirical method to determine the double-ionization thresholds has been used in the past [30,31] and was referred to as the "nth power rule," [30] meaning an approximately parabolic fit for double ionization. We have used n as fit parameters that was between 1.8 and 2.1 for the acenes benzene, naphthalene, anthracene, pentacene, and for coronene. However, this parameter was significantly lower (1.0–1.3) for pyrrole, furan, and selenophene. A small offset b was include in the fit function to take care of any remaining doubly charged ion signal due to second-order light, scattered light, or symmetric fragmentation.

The resulting double-ionization thresholds are summarized in Table I; the thresholds for the acenes have already been presented in Ref. [15] and have been compared to values from other experiments. Included in Table I are the exponents n of the fit using Eq. (1). Interestingly, there is a clear difference between the acenes and the molecules with a pentagonal structure. While the former have the expected exponent n of approximately 2, the latter have a significantly lower n.

As has been discussed previously [15], the photo-double- to photo-total-ionization ratio of acene parent ions scales with the length of the molecule at excess energies up to about 30 eV. This means, for instance, that the ratio for naphthalene is twice as large as the one for benzene. This scaling holds for the acenes from benzene to pentacene [15] when the molecules become longer. Coronene, however, is a molecule with a ring structure in two dimensions. Thus, it is interesting to find out whether the scaling model still applies.

TABLE I. Double-photoionization thresholds E^{2+} for benzene, naphthalene, anthracene, pentacene, pyrrole, furan, selenophene, and coronene given in eV. Also given is the exponent n used in the fit cf. [Eq.(1)].

Molecule	E^{2+}	n
Benzene	24.92(7)	1.82(9)
Naphthalene	21.39(11)	2.11(12)
Anthracene	20.07(17)	1.91(14)
Pentacene	18.62(21)	1.99(15)
Pyrrole	24.20(6)	1.23(6)
Furan	25.18(14)	1.32(5)
Selenophene	24.17(24)	0.99(17)
Coronene	18.8 (3)	2.0(2)

Figure 8 shows the ratio of doubly charged to all coronene parent ions as a function of excess energy and is compared to the corresponding helium ratio curve that serves as a model function described later. There are two features that deserve attention. First, the threshold region shows a very slow rise of the ratio, which, in general, is typical for molecules. Second, whereas the He ratio curve can be matched to the coronene data fairly well, it becomes apparent that there is another hump around 10 eV excess energy, as will be discussed later. Ignoring the threshold region, we have fit the He ratio curve to the coronene ratio curve between 13 and 33 eV, and we obtained an energy scaling factor of 1.05(3) with a ratio scaling of 6.68(10), which corresponds to an increase in the ratio relative to benzene of 6.21(10). In addition, we visually scaled our benzene ratio data to the coronene data (without scaling the energy) and obtained a factor of 6.15, as can be seen in Fig. 8. Both scaling factors are close to 6, which indicates the number of active benzene rings in the coronene molecule. Note that the "ring" in the center is actually a hole rather than a ring because it is created by the six surrounding rings.

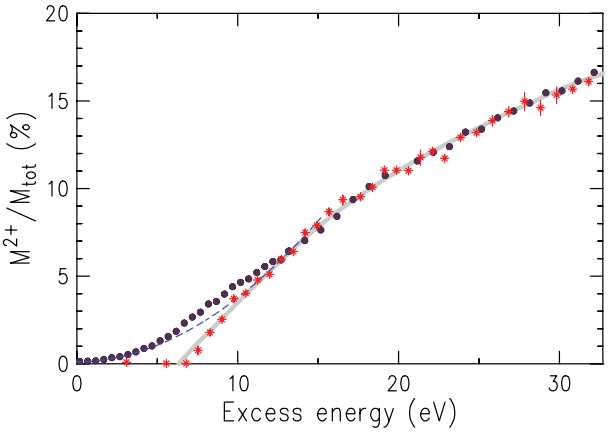

FIG. 8. (Color online) Ratio of doubly to all charged parent ions R_t as a function of excess energy of coronene (circles) and benzene (asterisks). The dashed line is the threshold-fit curve for coronene shown in Fig. 7(h). The gray solid line is the He ratio curve [32] scaled in width and height.

Thus, one can say that the relative photo-double-ionization probability corresponds to the number (or area) of active benzene rings.

B. Medium- and high-energy region

The energy behavior of the ratio R_s as a function of excess energy is presented in Fig. 9. The excess energy is defined as the energy above the double-ionization threshold of the corresponding molecule. The ratio curves exhibit a very similar behavior with a "heliumlike" rise up to about 30 eV, which is already known for the acenes [15]. The reason why we use the He photo-double- to photo-single-ionization ratio curve for comparison is that He is the simplest model system for photo-double-ionization with reliable data over an extended photon-energy range. It is known that the He photo-double-ionization process is mainly due to the knock-out mechanism at lower energies, which is the energy region in which we are interested, and only at higher energies does the shake-off mechanism make a significant contribution to the ratio. Therefore, helium serves here as a model system for the knock-out mechanism. Note that the shapes of the ratio curves of several other atoms (e.g., Li, Be, Na, Mg) are almost identical to the shape of the He ratio curve [33]. However, those experimental data are available only over a short energy range or have a lower accuracy than helium.

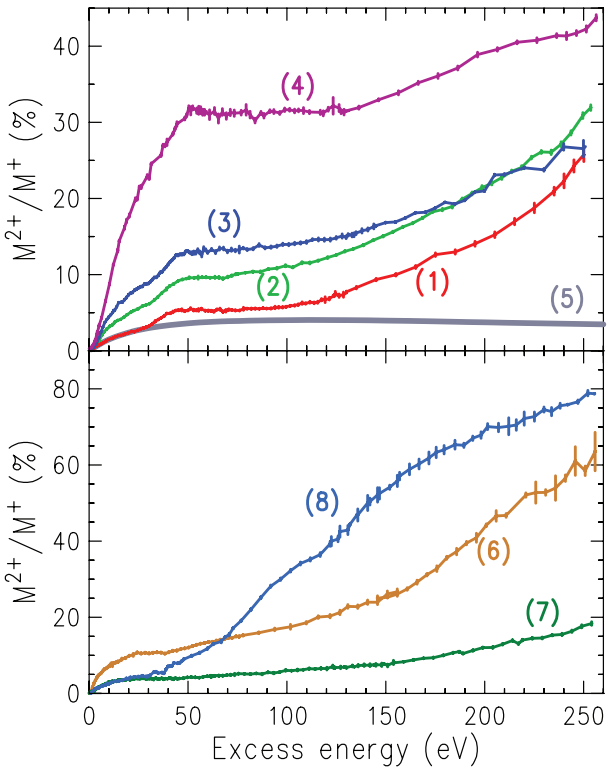

FIG. 9. (Color online) Ratio of doubly to singly charged parent ions R_s as a function of excess energy. The upper panel shows the ratios of partially deuterated benzene (1), naphthalene (2), anthracene (3), and pentacene (4). The gray curve (5) is the photo-double- to photo-single-ionization ratio of helium [32] scaled in height by 1.07 to match the benzene data at low energies [15]. The lower panel shows the ratios of pyrrole (6), furan (7), and selenophene (8).

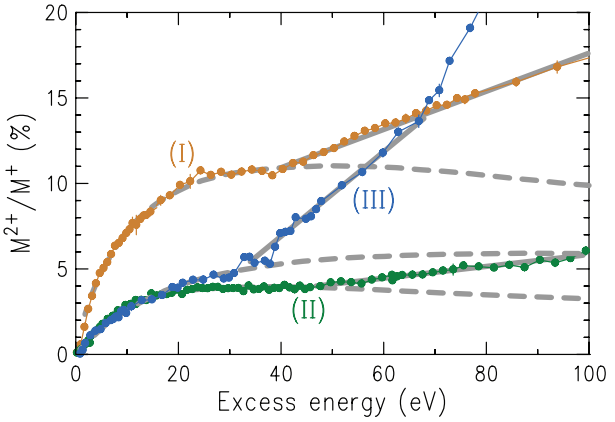

FIG. 10. (Color online) Ratio of doubly to singly charged parent ions R_s as a function of excess energy of pyrrole (I), furan (II), and selenophene (III). The gray dashed curves are He ratio curves [32] scaled in width and height. The gray solid curves are straight line fits to the high-energy part of the ratio data.

Figure 9 also shows that in contrast to atomic photo-double-ionization, the ratio keeps rising up to the carbon K shell, above which sequential photo-double-ionization dominates. Figure 9(b) demonstrates that the five-membered rings pyrrole, furan, and selenophene follow the same general behavior as the acenes. However, in their case the helium ratio curve has to be energy scaled to achieve a good fit to the molecular ratio, as can be seen in Fig. 10.

Above 30 eV the acenes show a distinct, broad hump in the ratio [16] before the ratio steadily increases. In contrast, pyrrole and furan do not show this hump but exhibit a perfect linear rise up to about 150 eV when the ratio starts to rise more steeply. This is partly true for selenophene as well, but the ratio rises linearly only up to about 70 eV before the ratio increases faster. The energy behavior of selenophene will be discussed in more detail in the next subsection.

Figure 10 visualizes the nearly perfect linear increase of the ratio above about 40 eV. The gray solid lines are linear fit curves to the ratio data above about 40 eV that match the ratio data very well. The linear increase of the ratio points to another double-ionization mechanism for aromatic molecules. The only case in which a linear increase of the ratio with photon energy has been predicted is for helium at high photon energies. In that case, the so-called "quasi-equal-energy sharing" mechanism results in a linear increase of the ratio [34]. At high enough photon energies, the two electrons can be regarded as almost free electrons that can be emitted with approximately the same energy in opposite directions [35]. While the helium case is not directly applicable to our case of aromatic molecules, it is conceivable that there is—similar to the helium case—a back-to-back emission of electrons with the same kinetic energy.

After subtracting the corresponding helium ratio curves $\mathcal{K}$, which represent the knock-out mechanism, from the molecules' ratios, we can clearly see an increased ratio starting at about 40 eV for partially deuterated benzene, naphthalene, and anthracene before it slightly decreases at about 70 eV followed by a linear increase of the ratio (Fig. 11) [16]. This linear increase, as discussed above, is also clearly visible for

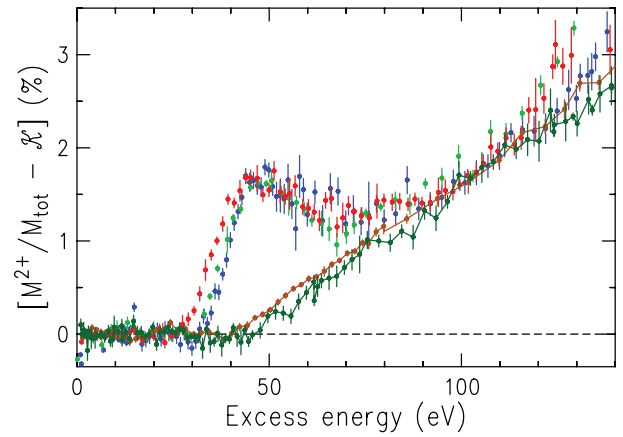

FIG. 11. (Color online) Ratio of doubly charged to all parent ions R_a after subtracting the contribution $\mathcal{K}$ of the knock-out mechanism using a scaled helium ratio curve. Partially deuterated benzene (red), naphthalene (green), and anthracene (blue) show a clear hump, whereas pyrrole (brown) and furan (dark green) only show a linear increase of the ratio above 40–50 eV. The pyrrole and furan ratios have been divided by 4 and 1.5, respectively, for easier comparison. These data have been presented over a shorter energy range in [16].

the ratios of pyrrole and furan that have been scaled to match the other ratios around 100 eV. With this scaling we also see that the slopes are very similar, and one can easily imagine that the linear increase of the ratio is also present in the acenes even though the hump is somewhat obscuring this feature. Above about 120 eV the ratio curves slowly diverge. Figure 11 also shows that the displayed ratios below 30 eV are close to zero, verifying that the helium ratio curves were a good fit. It is worthwhile to note that the linear increase of the ratio begins approximately where the hump in the ratio for the acenes is located (∼40 eV).

As discussed in Ref. [16], this hump is attributed to the formation of a two-electron pseudoparticle that one can regard as a Cooper pair. This formation is only possible if the de Broglie wavelength—corresponding to the kinetic energy of this Cooper pair—matches the C-C distance in the molecule, in which case the periodic structure of carbon atoms in the molecule facilitates the formation of the Cooper pair. Since the two-electron pseudoparticle is not directly in the plane of the carbon atoms but in an orbital located above and below that plane, one cannot expect a perfect match. Nevertheless, the ratio starts rising when the de Broglie wavelength matches the C-C distance. This photo-double-ionization mechanism is an additional way of creating a doubly charged ion and hence increases the ratio. With slightly increasing photon energy, the ratio continues to be elevated because any additional energy not necessary to form the pair will be used to eject that pair from the molecule [16]. At much higher photon energies, the discrepancy between the corresponding de Broglie wavelength and the C-C distance becomes too large to form the pair at all, and the hump in the ratio trails off. The size of a Cooper pair in a *conventional* superconductor is in the order of the coherence length, which can range from about 40 nm to several 100 nm. In *unconventional* superconductors, such as cuprates, the coherence length can be as small as 1–2 nm. The Cooper pair in benzene is limited to a space within about twice the C-C distance (i.e., the diameter of the molecule of 0.28 nm) and is, thus, much smaller than a Cooper pair in a conventional superconductor but not too much smaller than in unconventional superconductors.

We hypothesize that certain vibrational modes, not present in rings with an odd number of atoms, enables the formation of Cooper pairs similar to the electron-phonon coupling in conventional superconductors. This would explain why we do not observe any hump in the ratio for aromatic molecules with a pentagonal structure. However, this is still a subject of current investigations.

C. Special cases

In this section we will discuss selenophene and coronene, which behave slightly differently from the other molecules discussed here. First, we turn to selenophene, whose molecular structure is similar to that of furan (only oxygen is replaced by selenium), but it exhibits a more complicated energy dependence of the ratio of doubly to singly charged parent ions. In Fig. 12, we can see some "structure" in the overall rising ratio that reaches an impressive 80%%near the carbon K edge. We have analyzed the photon-energy dependence of the ratio based on our knowledge gained from the other molecules. After fitting a helium ratio curve below 60 eV photon energy (red curve in Fig. 12) and subtracting it from all selenophene ratio data, we see a linear increase of the remaining ratio up to about 95 eV when the ratio starts to rise even more steeply. After subtracting this linear increase (green dotted line in Fig. 12), it becomes evident that the following rise of the ratio can be described with another scaled helium ratio curve up to about 150 eV, above which a third helium ratio curve is needed to describe the data. After summing all four model curves, we obtain the dashed curve that fits the measured ratio very well. From the fits we have determined the onset of the linear ratio increase as 58.3(4) eV and the thresholds for the additional helium curves as 95.2(10) and 152.6(2) eV. The need for two more helium curves to describe the ratio data indicates the existence of two additional double-ionization thresholds. The first ionization threshold is the $1a_2$ orbital at 9.00 eV [36]. The first *double*-ionization threshold is typically at slightly

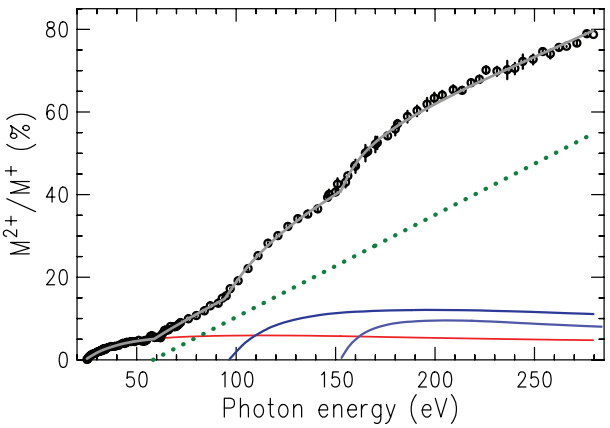

FIG. 12. (Color online) Ratio of doubly to singly charged parent ions R_s of selenophene (open circles). The solid and dotted lines are model fit curves described in the text. The gray dashed line along the data is the resulting model curve.

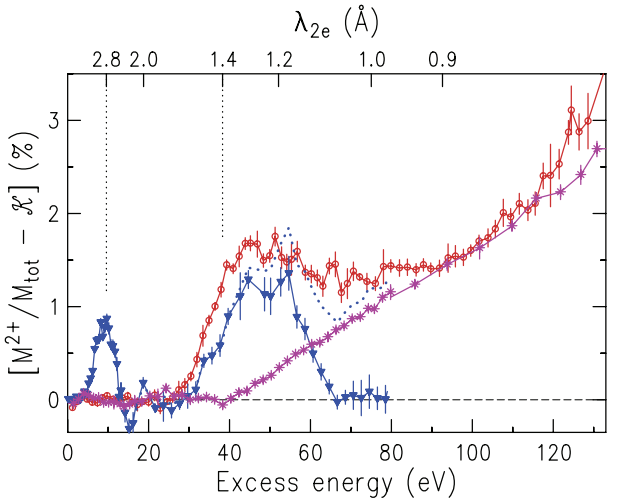

FIG. 13. (Color online) Ratio of doubly charged to all parent ions R_t of partially deuterated benzene (open circles), pyrrole (asterisks), and coronene (triangles) after subtracting the contribution $\mathcal{K}$ from the knock-out mechanism. The dotted line represents the coronene data sitting on top of the pyrrole curve (see text for details). The upper abscissa shows the de Broglie wavelength of a two-electron pseudoparticle.

less than a factor of 3 of the first ionization threshold. In our case, the double-ionization threshold is at 24.17 eV (see Table I) and the corresponding factor is 2.68. The next major orbital is near 57.7 eV [37], and applying the same factor yields a roughly estimated double-ionization threshold of 154.6 eV, which is close to the 152.6 eV that we obtained from the fit. The threshold at 95.2 eV is probably a combination of these outer and inner orbitals. We want to emphasize that this analysis was only possible due to the knowledge about the general energy dependence of the ratio of other simple molecules discussed above.

Another special case is coronene. As mentioned above and in Ref. [16], there is clearly a hump at about 10 eV corresponding to a de Broglie wavelength of 2.8 Å for a two-electron pseudoparticle (Fig. 13) that corresponds to twice the C-C distance. This mode is possible for coronene because of its larger size compared to benzene, where this hump does not occur. Although this mode is geometrically possible in benzene, the closed loop of the de Broglie wave would have a triangular shape due to its small size. Coronene, however, can easily support this mode on its outer rim as the molecule's diameter is three times larger than in benzene. We anticipate that pyrene, a molecule consisting of four benzene rings arranged in a rhombic shape, will also show a hump at twice the C-C distance.

We notice that the hump at 1.4 Å in coronene is slightly smaller than that in benzene. This is probably due to the fact that the hump in coronene is not sitting on a linearly increasing slope like the benzene hump is. As a simple test, we have added the pyrrole slope to the coronene hump, which is shown as a dotted line in Fig. 13 (likewise, one could subtract the pyrrole slope from the benzene hump). This procedure makes both humps more similar in size. We also note that there is no linear increase of the ratio below 80 eV excess energy in contrast to the other molecules discussed here.

V. CONCLUSION

We have measured the ratio of doubly to singly charged parent ions of various aromatic hydrocarbons from threshold to the carbon K edge using monochromatized synchrotron radiation. We have determined the first double-ionization thresholds for the molecules studied here, and also the two higher lying double-ionization thresholds for selenophene.

The photon energy dependence of the ratios has been analyzed, and we find three distinct mechanisms that contribute to the creation of doubly charged parent ions, which are summarized in Fig. 14. The ratios of partially deuterated benzene as well as pyrrole are used in this figure as representatives of six- and five-membered aromatic rings. The ratios can be partially described by a scaled helium ratio curve (area I) indicating the presence of the knock-out mechanism [15]. Benzene shows an additional hump in the ratio around 50 eV (area II) that is not present in pyrrole [16], and may thus serve as a model system for Cooper pair formation.

Above about 40 eV there seems to be a photo-double-ionization mechanism that causes part of the ratio to rise linearly, which is clearly visible for pyrrole but may be present also for benzene (area III in Fig. 14). In the case of benzene, one can also model the increase of the ratio above 50 eV by a fourth-order polynomial that describes the high-energy ratio. In both cases, the ratio starts to rise more steeply above about 130 eV (area IV). As far as we know, this energy does not correlate with any structures in the molecules. While the linear increase of the ratio indicates another photo-double-ionization mechanism, in which both electrons may be emitted back-to-back with

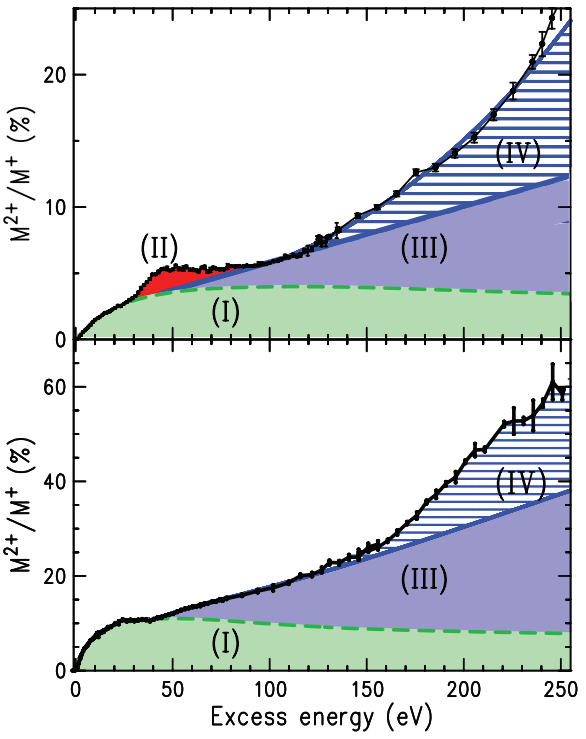

FIG. 14. (Color online) Ratio of doubly to singly charged parent ions R_s of partially deuterated benzene (top panel) and pyrrole (bottom panel). The differently colored (shaded) areas correspond to different double ionization mechanisms.

the same energy, there is still the unexplained "accelerated" increase (area IV) of the ratios at energies above 130 eV.

In future experiments, one could study the formation of Cooper pairs in other large molecules that may be even larger than coronene. In addition, one could study the effect of replacing some of the carbon atoms in the acenes by other elements. A particularly interesting molecule is a benzene ring with the isotope ^{14}C. This would explore the possible importance of vibrations in the formation of Cooper pairs in benzene and can be regarded as a related experiment to the classical studies on the isotope dependence in superconductivity of mercury [38,39].

ACKNOWLEDGMENTS

The authors wish to thank the staff of the Synchrotron Radiation Center for their excellent technical support. We are grateful to Dr. V. Kresin for many helpful discussions. K.C., B.R., and E.M. were supported by the REU program of the National Science Foundation. This work is based upon research conducted at the Synchrotron Radiation Center, University of Wisconsin–Madison, which was supported in the past by the NSF under Grant No. DMR-0537588 and is currently supported mainly by the University of Wisconsin–Madison.

[1] J. H. McGuire, N. Berrah, R. J. Bartlett, J. A. R. Samson, J. A. Tanis, C. L. Cocke, and A. S. Schlachter, J. Phys. B **28**, 913 (1995).
[2] R. Wehlitz, in *Advances in Atomic, Molecular, and Optical Physics*, edited by E. Arimondo, P. R. Berman, and C. C. Lin (Academic, New York, 2010), Vol. 58, pp. 1–76.
[3] T. Masuoka, J. Chem. Phys. **115**, 264 (2001).
[4] R. I. Hall, L. Avaldi, G. Dawber, A. G. McConkey, M. A. MacDonald, and G. C. King, Chem. Phys. **187**, 125 (1994).
[5] W. Vanroose, F. Martin, T. N. Resigno, and C. W. McCurdy, Science **310**, 1787 (2005).
[6] M. S. Deleuze, J.-P. Francois, and E. S. Kryachko, J. Am. Chem. Soc. **127**, 16824 (2005).
[7] D. A. Hagan and J. H. D. Eland, Rapid Commun. Mass Spectrom. **5**, 512 (1991).
[8] P. M. Mayer, V. Blanchet, and C. Joblin, J. Chem. Phys. **134**, 244312 (2011).
[9] S. Tobita, S. Leach, H. W. Jochims, E. Rühl, E. Illenberger, and H. Baumgärtel, Can. J. Phys. **72**, 1060 (1994).
[10] M. E. Wacks and V. H. Dibeler, J. Chem. Phys. **31**, 1557 (1959).
[11] T. Drewello, W. Krätschmer, M. Fieber-Erdmann, and A. Ding, Int. J. Mass Spectrom. Ion Process. **124**, R1 (1993).
[12] A. Reinköster, S. Korica, G. Prümper, J. Viefhaus, K. Godehusen, O. Schwarzkopf, M. Mast, and U. Becker, J. Phys. B **37**, 2135 (2004).
[13] P. N. Juranić, D. Lukić, K. Barger, and R. Wehlitz, Phys. Rev. Lett. **96**, 023001 (2006).
[14] S. Aksela, E. Nõmmiste, J. Jauhiainen, E. Kukk, J. Karvonen, H. G. Berry, S. L. Sorensen, and H. Aksela, Phys. Rev. Lett. **75**, 2112 (1995).
[15] T. Hartman, P. N. Juranić, K. Collins, B. Reilly, N. Appathurai, and R. Wehlitz, Phys. Rev. Lett. **108**, 023001 (2012).
[16] R. Wehlitz, P. N. Juranić, K. Collins, B. Reilly, E. Makoutz, T. Hartman, N. Appathurai, and S. B. Whitfield, Phys. Rev. Lett. **109**, 193001 (2012).
[17] K. Neumann, Superconductor Week **26**, 7 (2012).
[18] M. J. Rosseinsky and K. Prassides, Nature (London) **464**, 39 (2010).
[19] R. Mitsuhashi, Y. Suzuki, Y. Yamanari, H. Mitamura, T. Kambe, N. Ikeda, H. Okamoto, A. Fujiwara, M. Yamaji, N. Kawasaki, Y. Maniwa, and Y. Kubozono, Nature (London) **464**, 76 (2010).
[20] W. A. Little, Phys. Rev. **134**, A1416 (1964).
[21] V. Z. Kresin, V. A. Litovchenko, and A. G. Panasenko, J. Chem. Phys. **63**, 3613 (1975).
[22] *Organic Superconductivity*, edited by V. Z. Kresin and W. A. Little (Plenum, New York, 1990).
[23] R. K. Cole, F. K. Perkins, E. L. Brodsky, A. Filipponi, E. Korpella, D. C. Mancini, C. H. Pruett, D. J. Wallace, J. T. Welnak, and F. Zanini, Rev. Sci. Instrum. **60**, 2093 (1989).
[24] R. Reininger and A. R. B. de Castro, Nucl. Instrum. Methods Phys. Res. A **538**, 760 (2005).
[25] R. Wehlitz, D. Lukić, C. Koncz, and I. A. Sellin, Rev. Sci. Instrum. **73**, 1671 (2002).
[26] M. Stankiewicz, P. A. Hatherly, L. J. Frasinski, K. Codling, and D. M. P. Holland, J. Phys. B **22**, 21 (1989).
[27] S. Leach, J. H. D. Eland, and S. D. Price, J. Phys. Chem. **93**, 7583 (1989).
[28] A. P. Hitchcock, J. J. Neville, A. Jürgensen, and R. G. Cavell, J. Electron Spectrosc. Relat. Phenom. **88**, 71 (1998).
[29] A. P. Hitchcock and J. J. Neville, in *Chemical Applications of Synchrotron Radiation*, edited by T.-K. Sham, Advanced Series in Physical Chemistry Vol. 12A (World Scientific, Singapore, 2002), pp. 154–227.
[30] B. Brehm, U. Fröbe, and H.-P. Neitzke, Int. J. Mass Spectrom. Ion Proc. **57**, 91 (1984).
[31] F. H. Dorman and J. D. Morrison, J. Chem. Phys. **35**, 575 (1961).
[32] J. A. R. Samson, W. C. Stolte, Z.-X. He, J. N. Cutler, Y. Lu, and R. J. Bartlett, Phys. Rev. A **57**, 1906 (1998).
[33] J. B. Bluett, D. Lukić, S. B. Whitfield, and R. Wehlitz, Nucl. Instrum. Meth. Phys. Res. B **241**, 114 (2005).
[34] R. H. Pratt, T. Surić, and K. Pisk, J. Kor. Phys. Soc. **32**, 356 (1998).
[35] M. Ya. Amusia and E. G. Drukarev, J. Phys. B **36**, 2433 (2003).
[36] I. Reineck, C. Nohre, P. Lodin, R. Maripuu, B. Lindberg, L. Karlsson, K. Siegbahn, A.-B. Hörnfeldt, and S. Gronowitz, Chem. Secr. **22**, 209 (1983); I. Powis, I. L. Zaytseva, A. B. Trofimov, J. Schirmer, D. M. P. Holland, A. W. Potts, and L. Karlsson, J. Phys. B **40**, 2019 (2007).
[37] A. P. Hitchcock, G. Tourillon, and W. Braun, Can. J. Chem. **67**, 1819 (1989).
[38] E. Maxwell, Phys. Rev. **78**, 477 (1950).
[39] C. A. Reynolds, B. Serin, W. H. Wright, and L. B. Nesbitt, Phys. Rev. **78**, 487 (1950).